PHYSICAL REVIEW D **96,** 034018 (2017)

Total $\pi^+ p$ cross section extracted from the leading neutron spectra at the LHC

V. A. Khoze,[1,2] A. D. Martin,[1] and M. G. Ryskin[1,2]

[1]*Institute for Particle Physics Phenomenology, Durham University, Durham DH1 3LE, United Kingdom*
[2]*Petersburg Nuclear Physics Institute, NRC "Kurchatov Institute," Gatchina, St. Petersburg 188300, Russia*

(Received 17 May 2017; published 22 August 2017)

We use the very forward neutron energy spectra measured by the LHC forward experiment at 7 TeV to extract the $\pi^+ p$ total cross section at center-of-mass energies in the range 2.3–3.5 TeV. To do this, we have to first isolate the π-exchange pole in forward neutron production in pp collisions, by evaluating other possible contributions, namely, those from ρ and a_2 exchange, from both eikonal and enhanced screening effects, from migration, from neutron production by Δ-isobar decay and from diffractive nucleon excitations. We discuss the possible theoretical uncertainties due to the fact that the data do not exactly reach the π pole. We choose the kinematical domain where the pion contribution dominates and demonstrate the role of the different corrections which could affect the final result.

DOI: 10.1103/PhysRevD.96.034018

I. INTRODUCTION

The recent LHC forward (LHCf) measurements of leading neutron production at 7 TeV [1] have boosted the interest in attempts to extract the high-energy pion-proton cross section from these data; see for instance Refs. [2–4]. This, in turn, would allow new discriminative tests of the existing models of high-energy hadron interactions. Recall that at present the results of direct measurements of the $\pi^+ p$ cross sections are known only up to $\sqrt{s} = 25$ GeV [5]. In order to extend the pion-proton interaction energy range, various indirect methods for extraction of the πp cross section were proposed in the literature; see, for example, Refs. [6–9]. All these approaches are based one way or another on the assumption that one can reliably isolate the pion-exchange contribution in the corresponding processes. This topic has a long and checkered history (see, e.g., Refs. [10–16]).

The idea of using the inclusive leading neutron spectra in high-energy proton collisions for the separation of the pion-exchange contribution is to exploit the natural conjecture that, due to the small value of the pion mass, this term should play an important, or even, dominant role. The position of the pion pole is rather close to the physical region, and *if* it were possible to measure the cross section just at the pole, then undoubtedly we would deal with pure pion exchange. In particular, in such a case, absorptive corrections, caused by rescattering effects (see, for example, Refs. [17–19]) would be negligible, and the value of the so-called survival factor, S^2, of the rapidity gap associated with π exchange would be close to 1, $S^2 = 1$.

The problem is that we cannot reach the pole, which is outside the physical region, and the only way is to focus on a limited kinematic domain, located close to the π pole, and then to evaluate the size of the various corrections caused by the extrapolation to m_π^2. The main effects are:

(i) the contributions from the ρ and a_2 Regge trajectories which have intercepts higher than that for the pion; these terms will dominate when the momentum fraction carried by the leading neutron $x_L \to 1$,
(ii) absorptive corrections, that is a gap survival factor $S^2 < 1$,
(iii) leading neutrons produced in the decays of higher proton excitations such as $N^*(1440)$ or the Δ isobar,
(iv) migration [19] of the leading neutron due to baryon rescattering.

In Sec. II, we recall the expressions for the inclusive neutron cross section caused by the pion and the secondary Reggeon exchanges; then, in Sec. III, we consider the screening (or absorptive) corrections. In Sec. IV. we consider in detail those kinematic domains of the LHCf forward neutron data [1] which allow us to sufficiently isolate the π-exchange contribution so as to obtain reliable values of the πp total cross section. We find that to be closer to the pion pole and to minimize the transverse momentum effects we should choose LHCf data from the largest rapidity interval ($\eta > 10.76$) and to concentrate on the three bins of the neutron energy $E_n = 3.25 - 3, 3 - 2.75, 2.75 - 2.5$ TeV. In the largest x_L bin ($E_n = 3.5$–3.25 TeV), the experimental error and the possible contribution from ρ and a_2 trajectories are too large, while at lower x_L values, the pion has larger virtuality due to the longitudinal component of its momentum ($t_{\min} = (1 - x_L)^2 m_N^2 / x_L$), and the contribution from baryon rescattering, that is from migration, becomes non-negligible.

We present our results for $\sigma^{\rm tot}(\pi p)$ in Sec. V. In Sec. VI, we use the same formalism to describe the old lower-energy CERN-ISR data. Our conclusions and the outlook for applying the formalism to future leading neutron data are presented in Secs. VII and VIII, respectively.

 © 2017 American Physical Society

II. BORN-LEVEL CROSS SECTIONS

In this section, we evaluate the contributions to the cross section for forward neutron production in pp collisions coming from π, ρ, and a_2 exchanges and from baryon excitations of the protons.

A. Pion exchange

Neglecting absorptive effects, the contribution of Reggeized pion exchange to the inclusive neutron production reads

$$\frac{x_L d\sigma^{\pi}(pp\to nX)}{dx_L dq_t^2} = \frac{G^2_{\pi^+pn}(-t)}{16\pi^2(t-m_\pi^2)^2} F^2_{\pi N}(t)\sigma^{\rm tot}_{\pi p}(M_X^2)(1-x_L)^{1-2\alpha_\pi(t)}, \quad (1)$$

where $\alpha_\pi(t)=\alpha'_\pi(t-m_\pi^2)$ is the pion trajectory with slope $\alpha'_\pi=0.9$ GeV^{-2} and coupling $G^2_{\pi^+pn}/8\pi=13.75$ [20,21]. The formulas for the invariant mass M_X of the produced system X and of $-t$ are given by

$$M_X^2 = s(1-x_L), \quad (2)$$

$$-t = (1-x_L)^2 m_N^2/x_L + q_t^2/x_L, \quad (3)$$

where q_t is the neutron transverse momentum and m_N is the nucleon mass.

Here, we have retained in the Reggeon signature factor $\eta_\pi(t)$ only the denominator $1/(t-m_\pi^2)$, while the remaining t dependence is absorbed in the effective vertex form factor $F_{\pi N}(t)$. Below, we will use the non-Reggeized version of (1),

$$\frac{x_L d\sigma^{\pi}(pp\to nX)}{dx_L dq_t^2} = \frac{G^2_{\pi^+pn}(-t)}{16\pi^2(t-m_\pi^2)^2} F^2_{\pi N}(t)\sigma^{\rm tot}_{\pi p}(M_X^2)(1-x_L), \quad (4)$$

with a dipole parametrization of the form factor

$$F_{\pi N}(t) = 1/(1+(m_\pi^2-t)/0.71\ \text{GeV}^2)^2. \quad (5)$$

In such a form, (4), the interpretation of the result in terms of the πp cross section is more straightforward. It is possible to slightly modify the expression for $F_{\pi N}(t)$. This does not change the result noticeably. Moreover, since we work in the small $|t|$ domain, where the pion trajectory $\alpha_\pi(t)$ is close to zero, in both the Reggeized and non-Reggeized cases, we get practically the same result.

B. Secondary trajectories

Another contribution to the leading neutron spectrum is generated by the exchange of ρ and a_2 isovector trajectories. Due to their larger intercepts $\alpha_{\rho,a_2}(0)\simeq 0.5$, this contribution should dominate as $x_L\to 1$. We write the cross section arising for ρ exchange in a form analogous to (1)

$$\frac{x_L d\sigma^{\rho}(pp\to nX)}{dx_L dq_t^2} = |\eta(t)|^2 \frac{g_{\rm nf}^2 + g_{\rm sf}^2 q_t^2/4m_N^2}{16\pi^2(t-m_\rho^2)^2} F^2_{\rho N}(t)\sigma^{\rm tot}_{\rho p}(M_X^2)(1-x_L)^{1-2\alpha_\rho(t)}. \quad (6)$$

We assume "exchange degeneracy" (see, for example, Ref. [22]) between the ρ and a_2 exchanges. That is, the trajectory $\alpha_{a_2}(t)=\alpha_\rho(t)=0.54+\alpha' t$ (with $\alpha'=0.9\,\text{GeV}^{-2}$). Moreover, this means that the ρ and a_2 trajectories have the same residues and vertex form factors. The only difference is the signature factor

$$\eta(t) = \frac{1}{2}[1 \pm \exp(-i\pi\alpha_R(t))] \quad (7)$$

with a plus sign for a_2 exchange and a minus sign for ρ exchange ($R=\rho$, a_2). This means that when a_2 exchange is included we have to replace the first factor $|\eta(t)|^2$ in (6) by 1,

$$\frac{x_L d\sigma^{\rho+a_2}(pp\to nX)}{dx_L dq^2 t} = \frac{g_{\rm nf}^2 + g_{\rm sf}^2 q_t^2/4m_N^2}{16\pi^2(t-m_\rho^2)^2} F^2_{\rho N}(t)\sigma^{\rm tot}_{\rho p}(M_X^2)(1-x_L)^{1-2\alpha_\rho(t)}. \quad (8)$$

Here, $g_{\rm sf}$ and $g_{\rm nf}$ are the couplings corresponding to the processes where the neutron helicity is opposite (spin flip) to that of the incoming proton or the same (nonflip) as the proton helicity,[1] and we use $F_{\rho N}(t)=\exp(B_\rho t)$ with $B_\rho=2.3$ GeV^{-2}.[2]

Contrary to the pion-proton coupling G, which is known to rather good accuracy, there are no accepted values for the $\rho(a_2)$-nucleon vertices. The couplings $g_{\rm nf}$ and $g_{\rm sf}$ can be obtained from old Regge phenomenology, say, from Ref. [24], or alternately can be based on the vector meson dominance (VMD) model [25]. Since absorptive corrections were not accounted for in the old Regge phenomenological description, we prefer to use the VMD-based

[1]Recall that in the case of pion exchange we also have flip and nonflip contributions hidden in the factor $-t=q_t^2+q_L^2=q_t^2+t_{\rm min}+(1-x_L)q_t^2/x_L$, where the first term, q_t^2, corresponds to spin-flip production, while the second term, q_L^2, describes the nonflip process.

[2]This value is consistent with the slope observed for the RRP term in the triple-Regge analysis [23], accounting for the fact that part of the RRP slope comes from the Reggeon trajectory term $\alpha'_R\ln(1/(1-x_L))$.

values which are larger (see Table AA3 of Ref. [24]). That is, our estimate of the correction caused by the ρ, a_2 contribution may be considered "conservative." Finally, following the additive quark model, we assume that $\sigma(\pi p) = \sigma(\rho p) = \sigma(a_2 p)$.

C. Baryon excitations

For Δ-isobar production via pion and ρ and a_2 exchanges, we use formulas analogous to (1), (8) with couplings taken from Table AA3 of Ref. [24]. Since the different helicity states of the Δ are produced with different couplings, we account for the polarization effects in $\Delta \to n\pi$ decay.

Larger uncertainties may result from neutrons coming from the decays of the N^* resonances produced via the diffractive proton dissociation. Currently, there are no 7 TeV data on the cross section and polarization of the corresponding resonances. The only more or less relevant experimental cross section is the TOTEM result for low-mass ($M_X < 3.4$ GeV) proton dissociation, $\sigma^D_{\text{low}M} = 2.62 \pm 2.17$ mb [26]. Proton excitations with $M_X > 2$ GeV have a small probability to create a neutron with large x_L and small q_T; these states are decaying mainly into multiparticle systems with two or more pions. The main danger represents the contribution from the $M_X = 1.3$–1.8 GeV region. In our computations, we assume a nonpolarized (isotropic) decay with the branching ratio $\text{Br}(p^* \to n\pi^+) \simeq 1/3$ and the corresponding cross section of one proton excitation[3] to be 1 mb; see Sec. IV E.

III. SCREENING CORRECTIONS

Absorptive effects play an important role in processes where one particle carries away almost all of the beam energy; that is, its x_L is close to 1. This leads to the formation of a rapidity gap, since the remaining energy is not large enough to produce secondaries in the forward rapidity interval. However, any interaction of the fast particle will decrease the value of its x_L and thus diminish the cross section at large x_L. For example, these absorptive or screening corrections were responsible for the breaking of factorization, by about an order of magnitude, in diffractive dijet production at the Tevatron [27].

There are two types of absorptive corrections. These corrections are discussed in some detail in Ref. [19]. First, we have the effects caused by the inelastic interactions between the fast incoming proton (or leading neutron) and the target proton. The secondary particles from these interactions populate the rapidity gap separating the neutron from the other hadrons and carry away energy from the leading neutron. The corresponding correction is described by additional eikonal-like Pomeron exchanges, and we denote it as the "eikonal" gap survival factor S^2_{eik}. The corresponding diagrams are sketched in Fig. 1.

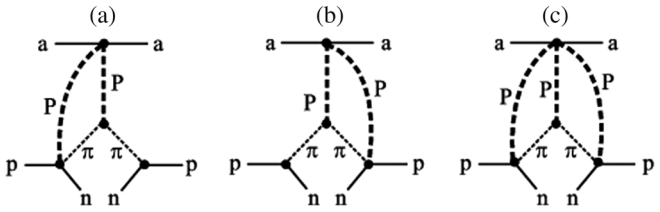

FIG. 1. Symbolic diagrams of the eikonal absorptive corrections to the cross section for the inclusive process $ap \to Xn$. In this paper, hadron a is a proton p, but in general, the target particle a can be any hadron. The extra lines denoted by P, which surround the triple-Regge interaction, represent multi-Pomeron exchanges between the leading hadrons.

Besides this, we have to consider an interaction (shown symbolically in Fig. 2) of the fast nucleon (proton or neutron) with the particles *within* the pion-target proton (or ρ-, a_2-proton) amplitude, that is in the remaining X system. This contribution could be enhanced due to a large multiplicity of particles in this system X. Therefore, we denote the corresponding damping factor as S^2_{enh}. The diagrams where an additional Pomeron screens the pion (ρ, a_2) propagator [such as shown in Fig. 3(b)] are also included in the S^2_{enh} factor, while the diagrams which describe an interaction of the pion (or ρ, a_2) with the system X [such as shown in Fig. 3(a)] are included in the π-proton ($\rho-$, a_2-proton) cross section.

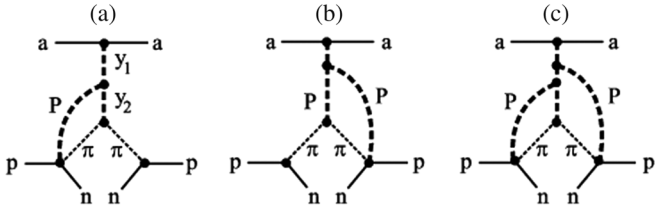

FIG. 2. Symbolic diagrams for the "enhanced" absorptive corrections to the cross section for the inclusive process $ap \to Xn$, which become important at very high energies. The extra lines denoted by P, which are coupled directly to the ingoing p or outgoing n, represent multi-Pomeron exchanges.

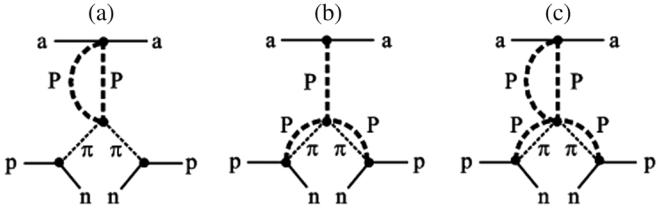

FIG. 3. Multi-Pomeron corrections to the Reggeons in the triple-Regge diagrams.

[3]Note that 2.6 mb corresponds to excitations of *both* of the initial protons.

A. Eikonal survival factor

To evaluate the most important (eikonal) screening correction, we follow the approach of Ref. [28] and work in impact parameter, b space. The "Born" cross section (1) can be written as (see Fig. 4 for the definition of the variables)

$$\frac{x_L d\sigma^\pi}{dx_L dq_t^2} = A \int \frac{d^2b_2}{2\pi} e^{i\vec{q}_t\cdot\vec{b}_2} F^\pi(b_2) \int \frac{d^2b_3}{2\pi} e^{i\vec{q}_t\cdot\vec{b}_3} F^\pi(b_3) \times \int \frac{d^2b_1}{2\pi} F^\sigma(b_1), \tag{9}$$

where all factors which do not depend on the transverse momentum are incorporated in the first factor A. The amplitudes $F^\pi(b_{2,3})$ are the Fourier conjugates of the pion-exchange amplitudes written in q_t space.. In particular, the spin nonflip amplitude reads

$$F^\pi_{\rm nf}(b) = \int \frac{d^2q_t}{2\pi} e^{-i\vec{q}_t\cdot\vec{b}} \frac{q_L F_{\pi N}(t)}{t - m_\pi^2} (1 - x_L)^{-\alpha_\pi(t)}, \tag{10}$$

where q_L is given by

$$q_L = \sqrt{-t_\parallel} = \sqrt{(m_N^2(1 - x_L)^2 + (1 - x_L)q_t^2)/x_L} \tag{11}$$

and m_N is the mass of the nucleon. Care should be taken in the case of a spin-flip amplitude since it depends on the *direction* of the transverse momentum $\vec{q}_t$. In practical terms, this means that the angular integration results not in a zero-order Bessel function $J_0(b_i q_t)$ but in the first order function $J_1(b_i q_t)$ (with $i = 2, 3$).

In the last integral, $F^\sigma(b)$ corresponds to the pion-proton amplitude. To calculate this amplitude, we use the same Pomeron-proton vertex form factor $F_{\rm Pom}$ and the same Pomeron trajectory slope, $\alpha'_{\rm Pom}$, as the ones used in the model [29] which allows a good description of the elastic proton-proton cross section measured by TOTEM [30] at $\sqrt{s} = 7$ TeV,

$$F^\sigma(b) = \int \frac{d^2k_t}{2\pi} e^{-i\vec{k}_t\cdot\vec{b}} F_{N-{\rm Pom}}(-k_t^2) F_{\pi-{\rm Pom}}(-k_t^2) x_L^{-k_t^2\alpha'_{\rm Pom}}, \tag{12}$$

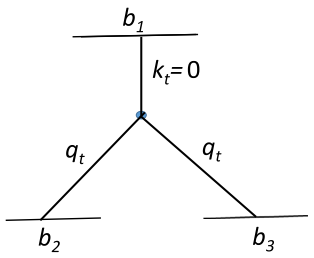

FIG. 4. The conjugate variables used in (9).

where the pion-Pomeron vertex form factor $F_{\pi-{\rm Pom}}(t) = \exp(B_\pi t)$ is parametrized by an exponent with slope $B_\pi = 2$ GeV^{-2} [31]. Note that there is no exponent $e^{i\vec{k}_t\cdot\vec{b}}$ in the last integral of (9) since this pion-proton amplitude is taken at $k_t = 0$.

Now, in the b representation, to account for the eikonal absorptive correction, we just have just multiply the integrand of (9) by the screening factors

$$S_{\rm eik}(\vec{b}_2 - \vec{b}_1) S_{\rm eik}(\vec{b}_3 - \vec{b}_1) = \exp(-\Omega(\vec{b}_2 - \vec{b}_1)/2) \exp(-\Omega(\vec{b}_3 - \vec{b}_1)/2), \tag{13}$$

where the proton-proton opacity Ω is taken from the model of Ref. [29] which reproduces well the elastic pp-cross section at 7 TeV. That is, we have to compute the integral

$$I^\pi(b_1) = \int \frac{d^2b}{2\pi} F^\pi(b) \exp(-\Omega(\vec{b} - \vec{b}_1)/2) \tag{14}$$

and to write the cross section as

$$\frac{x_L d\sigma^\pi}{dx_L dq_t^2} = A \int \frac{d^2b_1}{2\pi} F^\sigma(b_1) |I^\pi(b_1)|^2. \tag{15}$$

For the exchange of the ρ and a_2 trajectories, the gap survival factor $S^2_{\rm eik}$ is accounted for in a similar way.

Up to now, we described the calculation within the framework of a single-channel eikonal model which does not account for the internal structure of the incoming nucleon and for the possibility of nucleon excitations, $p \to N^*$, in the intermediate states.

On the other hand, the model [29], which we use, corresponds to a two-channel eikonal. That is, the nucleon wave function is described by a superposition of two Good-Walker [32] (GW) diffractive eigenstates. These are eigenstates with respect to the high-energy (Pomeron-exchange) interaction.[4] So, to implement the two-channel eikonal, we have to repeat the prescription described above for each combination of the GW eigenstates using the corresponding opacities Ω_{ij} where the indices $i, j = 1, 2$ denote the GW state in the fast (beam) and target nucleon, respectively.

B. Effect of the enhanced diagrams

The correction caused by enhanced screening can be calculated using the Abramovsky-Gribov-Kancheli Reggeon cutting rules [33]. These rules relate the cross section of high-mass diffractive dissociation with the value of absorptive correction.

Now, diffractive dissociation plays the role of the elastic cross section which was used to fit the eikonal proton opacity $\Omega(b)$ while calculating the $S^2_{\rm eik}$ survival factor (13). The

[4]There are no transitions between the different eigenstates caused by the Pomeron.

difficulty is that, unlike the elastic cross section, the experimental data on high-mass dissociation are quite scarce. Based on the preliminary TOTEM data [34], we assume that the cross section of single dissociation (integrated over the $M_X = 3.4$–1100 GeV mass interval) is $\sigma^{\rm SD} = 6.5$ mb[5] and that the mean t slope[6] is $B_{\rm dis} = 8.5$ GeV^{-2}.

Next, in order to estimate the contribution of the diagrams[7] of the type of Fig. 3(b), we use the Pomeron piece of the pion-nucleon cross section

$$\sigma(\pi N) = 13.63(s_{\pi N}/1\ {\rm GeV}^2)^{0.0808}\ {\rm mb}, \qquad (16)$$

in the Donnachie-Landshoff [35] parametrization, and the slope $B_{\pi N} = 6$ GeV^{-2} (see, e.g., Fig. 10 of Ref. [31]). Strictly speaking, both the cross section and the slope depend on x_L and the transverse momentum of the neutron. Here, we adopt representative values since the result is comparatively insensitive to the exact numbers. Indeed, due to the relatively small t slope (in comparison with that of the elastic scattering), the corresponding screening amplitude comes from the region of large impact parameters, b_t. The low b_t domain is already strongly suppressed by eikonal absorption (13), while at larger b_t the "tail" of the remaining enhanced screening amplitude is rather small. Therefore, this component of screening only weakly affects the final result. The same is valid for πN absorption, Fig. 3(b). Thus, it is sufficient to calculate the effective πN and enhanced opacities, $\Omega_{\rm enh}$, in a simplified way as

$$\Omega_{\pi N}(b) = \frac{\sigma(\pi N)}{2\pi B_{\pi N}} e^{-b^2/2B_{\pi N}}, \qquad (17)$$

$$\Omega_{\rm enh}(b) = \frac{\sigma^{\rm enh}}{2\pi B_{\rm dis}} e^{-b^2/2B_{\rm dis}}, \qquad (18)$$

where the effective cross section $\sigma^{\rm enh} = 14.1$ mb was recalculated[8] based on the TOTEM data as

$$\sigma^{\rm enh} = (\sigma^{\rm SD}/2)B_{\rm dis}/(\sigma^{\rm tot}/16\pi). \qquad (19)$$

Combining these results together, the opacity $\Omega(\vec{b} - \vec{b}_1)$ in (14) is replaced by the sum

$$\Omega = \Omega_{{\rm eik},ij}(\vec{b} - \vec{b}_1) + \Omega_{\pi N}(b) + \Omega_{\rm enh}(b) \qquad (20)$$

with $\Omega_{{\rm eik},ij}$ corresponding to the opacity in the interaction of the i and j GW components.

Let us examine this last modification in more detail. In fact, not all inelastic interactions populate the rapidity gap and reduce the neutron energy fraction, x_L. Part of the inelastic events have, from the beginning, no secondaries within the gap interval. First, there are events with dissociation of the target proton. It is evident that for target proton dissociation no new secondary particles are produced within the rapidity gap interval between the fast neutron and the remaining system X. Next, with some probability, $P(x_L)$, such a (moderately large) gap could be formed at the hadronization stage [36]. Assuming that, in a standard inelastic event, the neutron distribution is

$$\frac{dN}{dx_n} \simeq {\rm const}, \qquad (21)$$

we get $P(x_L) = 1 - x_L$. Therefore, we have to multiply the full opacity by $1 - P(x_L)$ and in addition multiply the eikonal opacity $\Omega_{{\rm eik},ij}$ by the factor

$$1 - \sigma^{\rm SD}/2\sigma_{\rm inel} = 1 - 6.5/2(98.7 - 24.9) = 0.956 \qquad (22)$$

to account for proton dissociation. So, finally, Eq. (20) is altered so that the full Ω in (14) becomes

$$\Omega = x_L(0.956\Omega_{{\rm eik},ij}(\vec{b} - \vec{b}_1) + \Omega_{\pi N}(b) + \Omega_{\rm enh}(b)). \qquad (23)$$

The absorptive factors for the leading Δ-isobar production and for the ρ- and a_2-exchange amplitudes are calculated in a similar way.

IV. ISOLATION OF π EXCHANGE IN LEADING NEUTRON LHCf DATA

We have seen that the inclusive leading neutron cross section is not *totally* given by the simple pion-exchange formula (1). Above, we have studied several other effects. We have enumerated contributions from ρ and a_2 exchanges and from neutrons coming from the Δ-isobar or from diffractive nucleon excitations decays, $N^* \to n\pi$. Next, we discussed absorptive corrections; indeed, we considered both eikonal and enhanced screening effects. So, in order to confront the LHCf data on forward neutrons, we should explore the kinematic domains of the data where (a) π exchange dominates and (b) the original Born amplitude is minimally modified.

A. Form factor of the πN vertex

Even for pion exchange, the form factor of the pion-nucleon vertex is poorly known. This is not a big problem when we are working close to the pion pole, say, using the

[5]The small value, 6.5 mb, is explained by the smallness of the triple-Pomeron vertex and strong eikonal absorption.

[6]In the three measured M_X mass intervals, the values of slope were found to be $B_{\rm dis} = 10.1$, 8.5, 6.8 GeV^{-2} [34].

[7]The significant role of these diagrams was emphasized in Ref. [16].

[8]We do not include here the cross section of low-mass dissociation, since in the case of a two-channel eikonal the low-mass dissociation is reproduced by the nonzero dispersion of the individual GW component cross sections σ_{ij} (see Ref. [29] for the details). We take only a half of the whole $\sigma^{\rm SD}$ since the experimental number accounts for the dissociation of both protons, while here we have to consider high-mass dissociation of the target proton only.

LHCf data for neutron rapidities $\eta > 10.76$ and looking for the neutrons with $E_n = 3.25$–2.5 TeV which correspond to a mean $-t = 0.02$–0.08 GeV^2, respectively. In this case, a variation of the slope of the form factor, $F(t) = e^{Bt}$, by $\delta B = \pm 1$ GeV^{-2} will lead to a $2\delta B(m_\pi^2 - t) \sim \pm(8-20)\%$ variation of the result, respectively. Already at this stage, we see that at lower x_L the theoretical uncertainty increases, and it is safer not to go below $x_L = 0.75$ (that is, the $E_n = 2.75$–2.5 TeV bin). The situation becomes much worse for a smaller rapidities. In particular, for the case of $\eta = 8.99$–9.22, the mean $|t|$ is about 0.5 GeV^2 leading to up to a factor of 0.4 to 2.7 uncertainty.[9] Therefore, below, we consider only the largest $\eta > 10.76$ rapidity interval.

Recall that in our calculation we used non-Reggeized pion exchange. If instead the Reggeized version of (1) was implemented with a vertex form factor $F(t) = \exp(1.5(t - m_\pi^2))$ [where $(t - m_\pi^2)$ is in GeV^2], the results change only by $\pm 2\%$ (where $+2\%$ is for the $E_n = 2.75$–2.5 TeV bin).

B. Screening effects

Besides this, for larger $|t|$, the screening effects become stronger. For the $\eta = 8.99$–9.22 interval, the full survival factor is rather small, namely $S^2 = \langle e^{-\Omega} \rangle \simeq 0.032$–$0.075$; that is, $\langle \Omega \rangle \sim 3$. So, due to the exponential dependence, even a moderate theoretical uncertainty in the calculation of Ω could strongly influence the result. For larger rapidities $\eta > 10.76$ and $x_L > 0.75$, the major contribution comes from relatively large impact parameters where the nucleon is not so black, that is, where the optical opacity Ω is not large. Here, for $E_n = 3.25$–2.5 TeV, the mean survival factor is, respectively, $S^2 = 0.45$–0.3, and within an accuracy of (5%–10)%, we can rely on the calculation of the absorptive corrections. Indeed, using, instead of the two-channel eikonal model [29], a one-channel approach with the opacity taken just from the experimental data multiplied by the "semienhanced" factor $C = 1.3$ [37] to account for possible N^* intermediate states (and neglecting the Re/Im ratio[10]), we obtain a cross section larger by about 6%–12% only.

Neglecting completely enhanced screening enlarges the cross section by about 10%–20%, while replacing the Donnachie-Landshoff Pomeron contribution to the pion-nucleon cross section by $\sigma_{\pi N} = 26$ mb, we obtain a result smaller by 4%–8%. These numbers correspond to the $E_n = 3.25$–2.5 TeV interval.

C. ρ, a_2 and Δ effects

The contribution coming from the secondary ρ and a_2 Reggeons calculated using the couplings obtained in Ref. [24] based on the vector meson dominance model is rather large in the highest x_L bin (with E_n in the 3.5–3.25 TeV bin and $\eta > 10.76$). Assuming the equal meson-proton cross sections ($\sigma(\rho p) = \sigma(a_2 p) = \sigma(\pi p)$), it amounts to 37% of the pion-exchange term. However, in three bins with lower E_n, the contribution of the ρ and a_2 diagrams decreases to (12–9)%. Bearing in mind large experimental error (46%) and the large admixture of the ρ and a_2-exchange processes in the highest x_L bin, we prefer not to use this kinematic region for extracting the high-energy pion-proton cross section.

The contribution from the Δ-isobar decay in this domain is practically negligible. Calculating the cross section of Δ production using the couplings from Ref. [24], after the decay, we get less than a 1.1%–2.5% correction.

D. Migration

The next problem is migration. After an additional soft interaction, the fast nucleon may change its momentum and "migrate" from one kinematical bin to another. This possibility was considered in detail in Ref. [19] where it was shown that for low $q_t < 0.1$ GeV migration practically does not affect the neutron spectra at $x_L > 0.75$ and thus could be neglected in the region of interest.[11]

E. Low-mass diffractive proton excitations

A more serious problem arises from neutrons produced in the decay of low-mass diffractive proton excitations, $N^* \to n\pi$. At $\sqrt{s} = 7$ TeV, the TOTEM result [26] for the cross section of low-mass proton dissociation is $\sigma^{\rm D}_{{\rm low}M} = 2.6 \pm 2.2$ mb, with $M_X < 3.4$ GeV; this measurement corresponds to allowing both protons to diffract. That is, the cross section of *one* proton dissociation is about 1.5 mb. Note that part of this cross section is already included in the pion-exchange contribution. Indeed, keeping the elastic component in the total pion-proton cross section, we include the $pp \to (n + \pi^+) + p$ process where in almost the whole essential kinematic region the mass of the $n\pi$ system is less than 3.4 GeV. Accounting for the screening corrections, this Drell-Hiida-Deck [38] contribution is equal to

$$\sigma^{\rm DHD} = 0.026\sigma_{\rm el}(\pi p) \sim 0.2\text{–}0.3 \text{ mb}. \qquad (24)$$

Thus, we still have more than 1 mb of diffractive proton dissociation which, in its decay, could produce leading

[9]Besides this, at larger q_t values, the relative contribution of the ρ, a_2 trajectories increases since the corresponding vertices have a very large spin-flip component which is proportional to q_t.

[10]The real part of the elastic amplitude was accounted for in our calculations of the rescattering corrections. It enlarges the final cross section by less than 1%.

[11]One rescattering gives about 1.6%–7.1% contribution in the $E_n = 3.25$–2.5 region. Note that after the S^2 absorption is taken into account only the large b_t contributions survive, and the mean number of rescatterings, $\langle \nu \rangle = \langle \Omega \rangle$, is less than 0.3 for the $E_n = 3.25$–3 TeV bin and less than 0.6 for the $E_n = 2.75$–2.5 TeV bin.

TABLE I. The second and third columns show, respectively, the cross sections (μb/TeV) for leading neutrons as measured by LHCf [1] and the contribution $\Delta\sigma^{\rm diff}$ coming from the decay of low-mass proton excitations, $N^* \to n\pi$, calculated as described in Sec. IV E. The $i = \pi, \rho + a_2, \Delta$ columns are the ratios $R^i = (d\sigma^i/dE_n)/\sigma(\pi^+ p)$ of the calculated inclusive cross section to the total pion-proton cross section. The ratios presented here are measured in inverse TeV and multiplied by a factor of 1000, so that the LHCf result divided by R^i gives the value of $\sigma(\pi^+ p)$ in mb; for example, for the 3–2.75 TeV bin, accounting for π exchange only, we obtain $\sigma(\pi^+ p) = 282/5.53 \simeq 51$ mb; since the π fraction is 88% (see Table II), this results in the true $\sigma_{\rm tot}(\pi^+ p) \simeq 45$ mb. Finally, the "Migr" column shows the effect of fast neutron rescattering (that is, migration of the leading neutron). The last column shows the mean value of the momentum fraction carried by the pion in the case of the pion-exchange contribution.

E_n (TeV)	LHCf data	$\Delta\sigma^{\rm diff}$	π	$\rho + a_2$	Δ	Migr (%)	$\langle 1 - x_L \rangle$
3.5–3.25	232 ± 106	58	2.41	0.87	0.01	0.2	0.047
3.25–3	249 ± 78	9.6	5.62	0.66	0.06	0.6	0.109
3–2.75	282 ± 48	1.6	5.53	0.50	0.09	1.7	0.177
2.75–2.5	298 ± 34	0.4	3.75	0.34	0.09	5	0.247

TABLE II. The third column is the $\pi^+ p$ total cross section (mb) extracted from the LHCf leading neutron data $d\sigma/dE_n$ (μb/TeV) shown in the second column. The result for the first E_n bin is not reliable (see the huge error bar) and is shown only for completeness. The fourth column is the mean pion-proton energy corresponding to the particular E_n bin. The value of the $\pi^+ p$ cross section (mb) obtained from the extrapolation of a simple Regge pole fit [35] and from the Compete fit [40] to lower-energy hadron-hadron cross section data are shown for comparison in the fifth and sixth columns, respectively. The last two columns show the relative contribution of the pion-exchange process to the total leading neutron cross section and the pion-exchange gap survival factor, respectively.

E_n (TeV)	LHCf data	$\sigma_{\rm tot}(\pi p)$	$\sqrt{s_{\pi p}}$ (TeV)	$\sigma^{\rm Reg}$	$\sigma^{\rm Comp}$	π fraction	S^2_π
3.5–3.25	232 ± 106	52.7 ± 32.1	1.52	44.6	60.1	0.55	0.56
3.25–3	249 ± 78	$\mathbf{37.5 \pm 12.2}$	**2.31**	47.7	65.9	0.85	0.44
3–2.75	282 ± 48	$\mathbf{45.0 \pm 7.7}$	**2.94**	49.6	69.4	0.88	0.36
2.75–2.5	298 ± 34	$\mathbf{67.9 \pm 7.7}$	**3.48**	50.9	71.9	0.85	0.32

neutrons. Unfortunately, there is insufficient information at the LHC energies; we do not know the M_X mass distribution, the t slope of the low-mass dissociation, nor the possible polarization of the N^* resonances. Looking at the lower-energy data, we assume that the dominant contribution comes from the region of $M_X \sim 1.7$ TeV and that the N^* system is produced with the same slope as that in elastic pp-scattering; that is, $B_{\rm dis} = 20$ GeV^{-2} [30].

At large values of the neutron $x_L > 0.75$, the main contribution arises from the two-body $N^* \to n\pi^+$ decay. For higher multiplicity, it becomes difficult to allow for such a large neutron momentum fraction. We assume a nonpolarized decay with the branching ratio[12] Br $\simeq 1/3$.

The cross sections that we find, assuming $\sigma(N^*) = 1$ mb, can be rather large; see the third column of Table I. In the highest $E_n = 3.5$–3.25 TeV bin, they could account for up to 25% of the leading neutron cross section. For the next three bins, this contribution becomes negligible in comparison with the experimental error bars of the LHCf data.

V. $\pi^+ p$ CROSS SECTION FROM LHCf LEADING NEUTRON DATA

We use the different contributions to forward neutron production in pp collisions described above, together with LHCf data [1], to extract the $\pi^+ p$ total cross section at various energies $\sqrt{s_{\pi p}}$. The results are shown in Table II. We show only the errors coming from the experimental error bars. The uncertainties arising from the theoretical approach were discussed in Sec. IV, and the sizes of the individual contributions are shown in the central part of Table I. As expected from Sec. IV, we see that the result for the highest E_n bin (that is, the bin with the highest x_L, which corresponds to the lowest pion-proton energy $\sqrt{s_{\pi p}}$) is not reliable and is shown only for completeness. On the other hand, we expect better theoretical accuracy for the next three experimental E_n bins where we have a larger fraction of π exchange. It is clearly seen from Table II and Fig. 5 that the pion-proton cross section increases with energy; however, the uncertainties are rather large.

[12]The $N^* \to n\pi^+$ branching ratio Br $\simeq 1/3$ comes from about 50% $N^* \to N\pi$ branching, with the other 50% due to the $N\pi\pi$ and $\Delta\pi$ decay channels (these are the typical branching ratios for N^* resonances in the 1400–1700 MeV region [5]). Finally, a factor 2/3 comes from the isotopic spin factor $\mathrm{Br}(p^* \to n\pi^+)/\mathrm{Br}(p^* \to p\pi^0) = 2$. Note that the resulting cross section $\sigma(N^* \to n\pi^+) \simeq 0.33$ mb is in agreement with the lower-energy data [39] ($\sigma \sim 0.3$ mb) assuming that the flat energy dependence continues up to LHC energies.

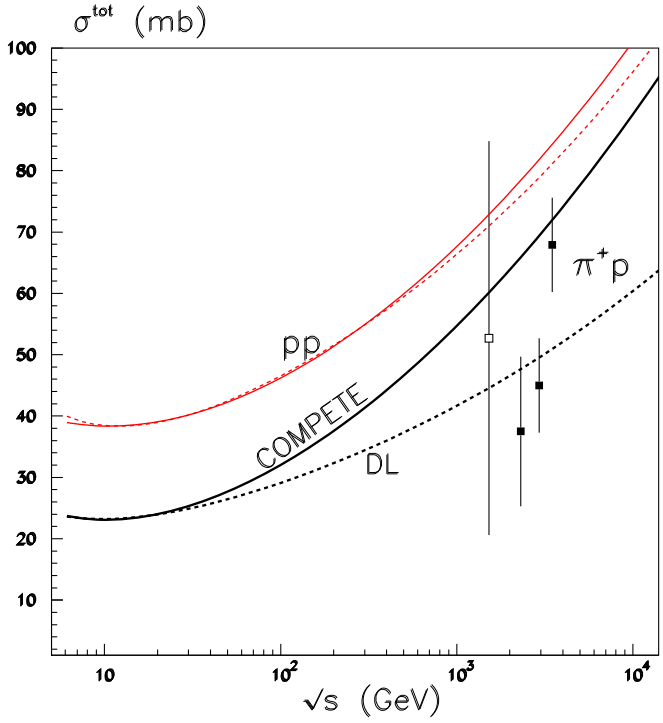

FIG. 5. The four values of $\pi^+ p$ total cross section that we extract from the LHCf data on leading neutrons [1], compared with expectations based on fits to lower-energy hadron-hadron total cross section data parametrized by two Regge poles, DL [35], or using the COMPETE parametrization [40]. Note that the results of both parametrizations coincide in the region of the existing πp cross section data, that is, for $\sqrt{s} < 25$ GeV. For reference, the upper two (red) curves are the corresponding descriptions of the pp total cross section. Recall that the error bars shown here reflect the experimental uncertainties only. The possible theoretical uncertainties are discussed in detail in the main body of paper; see Secs. II–IV.

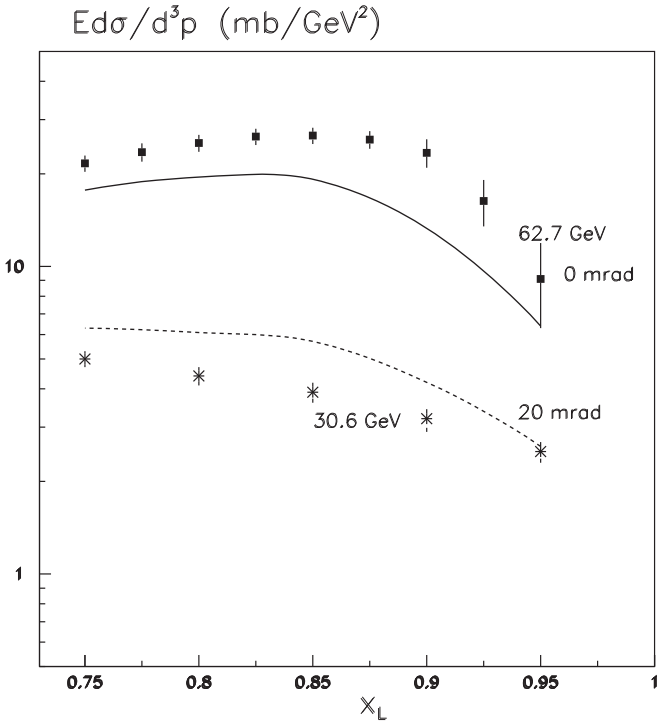

FIG. 6. The description of the CERN-ISR leading neutron data [41,42].

Figure 5 compares the values of $\sigma_{\rm tot}(\pi p)$ extracted from the LHCf data with two predictions based on extrapolations of fits to lower-energy hadron-hadron cross sections, shown by the lower two curves labelled DL [35] and COMPETE [40]. The large error bars do not allow us to decide between the two extrapolations. For reference, we also show, by the upper two curves, the DL and COMPETE descriptions of the total pp cross section.

The values of the $\pi^+ p$ cross section that we obtain are smaller than those of Ref. [4] extracted from the same LHCf data but at a lower rapidity interval $8.99 < \eta < 9.22$. Recall, however, that at lower rapidities we deal with relatively large $q_t \sim 0.6$ GeV, that is, with $|t| \sim 0.4$ GeV^2, where the uncertainty in the form factor can appreciably change the result. Moreover, nothing is said in Ref. [4] about the effects of migration, proton diffractive dissociation, and the enhanced absorptive corrections. The role of all these effects was described in Sec. IV above, and, since for $\eta > 10.76$ we work much closer to the π pole, we believe our results, shown in Table II and Fig. 5, are more reliable.

Nevertheless, one has to remember that the extraction of the pion-proton cross section from leading neutron inclusive data is not so straightforward. To describe the full "kitchen" of effects hidden in this procedure is one of the goals of our paper.

VI. DESCRIPTION OF THE CERN-ISR DATA

In order to check the quality of our approach, in Fig. 6, we use the same formalism (as that we used to describe the LHCf data) to calculate the leading neutron cross sections measured in the CERN-ISR energy range for $\sqrt{s}_{pp} =$ 30.6–62.7 GeV [41,42]. The description of the data of the two experiments is puzzling. We underestimate the data obtained at zero angle ($q_t = 0$) but overestimate the data obtained at 20 mrad. Note, however, that the two groups of data come from different experiments and reveal some inconsistency. It is hard to provide the steep q_t dependence that is needed to reconcile both data sets[13] with reasonable slopes of the vertex form factors $F(t)$.

Moreover, contrary to the zero degree case, the 20 mrad curve in Fig. 6 is the *minimal* prediction. It includes only the π, ρ, and a_2 contributions and neglects the $p \to N^* \to n + X$ dissociation which in some papers

[13]The energy dependence in each experiment was rather weak, and the data are consistent with the scaling behavior; that is, at a fixed q_t and x_L, the cross section does not depend on $\sqrt{s}$.

(e.g., Refs. [39,43]) was described completely via the Deck process [38].[14]

It was suggested by Kopeliovich *et al.* [16] that most probably the data at $q_t = 0$ have unreliable normalization. On the other hand, Kaidalov's group trusts the zero angle data more; recall that in Ref. [42] it was emphasized that in the first experiment [41] the background was rather high. Our prediction is somewhere in between the two data sets. Recall that, in comparison with the LHCf data, the CERN-ISR data are at much lower energies, where the secondary Reggeon contributions are not negligible and other effects not discussed here may be present; nevertheless, the accuracy of our description should still be reasonable.

VII. CONCLUSION

We discuss the different contributions to the leading neutron inclusive spectra of LHCf [1]. Besides pion exchange, as $x_L \to 1$ an important role is played by the ρ and a_2 trajectories. In addition, we have to account for the neutrons coming from diffractive dissociation such as $pp \to (n\pi^+) + p$ and for the final state rescattering of the leading baryon, which leads to migration of the leading neutron from one to another kinematical bin. Nevertheless, there exists a *small* kinematic domain ($x_L \sim 0.75$–0.9 and $q_t < m_\pi$) where the pion pole dominates[15] and the π-exchange amplitude provides more than 80% of the observed cross section. The data collected in three bins in this region can be used to extract the value of the $\pi^+ p$ total cross section; see Table II and Fig. 5.

Recall that, even here, we have to account for the absorptive corrections (that is, include a gap survival factor S^2) which suppresses the original (Born) cross section by more than a factor of 2 (see the last column of Table II). However, in this small q_t region, the value of S^2 can be *reliably* calculated with good accuracy based on the data for elastic pp-scattering which allow a good determination of the proton optical density [that is, the opacity, $\Omega(b)$]. Of course, there is some uncertainty depending on the particular model used to describe the differential elastic cross section, but as we demonstrated in Sec. IV B, this uncertainty is not too large.

Actually, the main aim of our paper is not just to extract the pion-proton cross section but rather to explain all the subtleties hidden in the procedure in order to give an understanding of the possible theoretical uncertainties. One outcome is that it is indeed possible to find a kinematic region where the pion pole dominates. However, even in this case, it is critical to account for the S^2 absorptive correction, which, as mentioned above, appreciably affects the value of the cross section.

Within the experimental error bars, the results obtained for $\sigma_{\rm tot}(\pi p)$ are consistent with the extrapolation given by Donnachie-Landshoff [35] or COMPETE [40] parametrizations. The present indications are that the πp cross section rises with energy steeper than in the proton-proton case.

VIII. OUTLOOK

The present leading neutron data, and hence our determination of $\sigma_{\rm tot}(\pi^+ p)$ in the few TeV energy region, are not yet sufficiently accurate to be very informative. But as the experimental statistics improve, it should be possible, with the framework we discussed, to make a good determination of the high-energy dependence of $\sigma_{\rm tot}(\pi^+ p)$. Moreover, when the 13 TeV data become available, it will be possible to extend the energy reach of the measurements and to enter the region which can distinguish between the extrapolations (for example, Refs. [35,40]) from lower energies.

To obtain a more precise result and to better fix the parameters, it would be valuable to measure the q_t dependence of the leading neutron spectra. As discussed in Ref. [9], this could be achieved in a CMS measurement with the zero degree calorimeter. Engaging the forward shower counters (FSC) [44] would allow the suppression of the contribution arising from low-mass dissociation of the beam proton.

On the other hand, in the common runs of LHCf with ATLAS, it will be possible to study the low-mass diffractive proton dissociation, $p \to N^* \to n + X$, contribution and to exclude this component from the inclusive (nondiffractive) neutron cross section. Again, FSC analogous to Ref. [44] will allow a better selection of low-mass dissociation.

Moreover, ATLAS could measure the *distribution of secondaries* in the events containing a leading neutron. In this way, we have a chance to study not only the value of $\sigma_{\rm tot}(\pi^+ p)$ but also the inclusive cross sections in the $\pi^+ p$ collisions as well.

ACKNOWLEDGMENTS

We are grateful to Takashi Sako and Sergey Ostapchenko for useful discussions. M. G. R. thanks the IPPP at Durham University for hospitality, and V. A. K. thanks the Leverhulme Trust for an Emeritus Fellowship. The research of M. G. R. was supported by RSCF Grant No. 14-22-00281.

[14]However, without accounting for the gap survival factor S^2.

[15]Essentially only in three bins of over the 40 bins of data collected by the LHCf [1].

[1] O. Adriani *et al.* (LHCf Collaboration), Phys. Lett. B **750**, 360 (2015).
[2] V. A. Petrov, R. A. Ryutin, and A. E. Sobol, Eur. Phys. J. C **65**, 637 (2010).
[3] B. Z. Kopeliovich, H. J. Pirner, I. K. Potashnikova, K. Reygers, and I. Schmidt, Phys. Rev. D **91**, 054030 (2015).
[4] R. A. Ryutin, Eur. Phys. J. C **77**, 114 (2017).
[5] C. Patrignani *et al.* (Particle Data Group), Chin. Phys. C **40**, 100001 (2016).
[6] P. Soding, Phys. Lett. **19**, 702 (1966).
[7] M. G. Ryskin and Y. M. Shabelski, Yad. Fiz. **61**, 89 (1998); Phys. At. Nucl. **61**, 81 (1998).
[8] J. Breitweg *et al.* (ZEUS Collaboration), Eur. Phys. J. C **2**, 247 (1998).
[9] A. E. Sobol, R. A. Ryutin, V. A. Petrov, and M. Murray, Eur. Phys. J. C **69**, 641 (2010).
[10] G. F. Chew and F. E. Low, Phys. Rev. **113**, 1640 (1959).
[11] C. Goebel, Phys. Rev. Lett. **1**, 337 (1958).
[12] S. D. Drell, Phys. Rev. Lett. **5**, 278 (1960).
[13] K. G. Boreskov *et al.*, Sov. J. Nucl. Phys. **15**, 203 (1972); **19**, 565 (1974); **21**, 84 (1975).
[14] B. Z. Kopeliovich, I. K. Potashnikova, I. Schmidt, and J. Soffer, Phys. Rev. D **78**, 014031 (2008).
[15] Nikolai N. Nikolaev, W. Schafer, A. Szczurek, and J. Speth, Phys. Rev. D **60**, 014004 (1999).
[16] B. Z. Kopeliovich, I. K. Potashnikova, and I. Schmidt, Acta Phys. Pol. B Proc. Suppl. **8**, 977 (2015).
[17] N. N. Nikolaev, J. Speth, and B. G. Zakharov, arXiv:hep-ph/9708290.
[18] U. D'Alesio and H. J. Pirner, Eur. Phys. J. A **7**, 109 (2000).
[19] A. B. Kaidalov, V. A. Khoze, A. D. Martin, and M. G. Ryskin, Eur. Phys. J. C **47**, 385 (2006).
[20] V. G. J. Stoks, R. Timmermans, and J. J. de Swart, Phys. Rev. C **47**, 512 (1993).
[21] R. A. Arndt, I. I. Strakovsky, R. L. Workman, and M. M. Pavan, Phys. Rev. C **52**, 2120 (1995).
[22] P. D. B. Collins, *An Introduction to Regge Theory and High Energy Physics* (Cambridge University Press, Cambridge, England, 1977).
[23] A. B. Kaidalov, V. A. Khoze, Yu. F. Pirogov, and N. L. Ter-Isaakyan, Phys. Lett. **45B**, 493 (1973); R. D. Field and G. C. Fox, Nucl. Phys. **B80**, 367 (1974).
[24] A. C. Irving and R. P. Worden, Phys. Rep. **34**, 117 (1977).
[25] C. Michael, Springer Tracts Mod. Phys. **55**, 174 (1970).
[26] G. Antchev *et al.* (TOTEM Collaboration), Europhys. Lett. **101**, 21003 (2013).
[27] A. B. Kaidalov, V. A. Khoze, A. D. Martin, and M. G. Ryskin, Eur. Phys. J. C **21**, 521 (2001).
[28] E. G. S. Luna, V. A. Khoze, A. D. Martin, and M. G. Ryskin, Eur. Phys. J. C **59**, 1 (2009).
[29] V. A. Khoze, A. D. Martin, and M. G. Ryskin, Eur. Phys. J. C **74**, 2756 (2014).
[30] G. Antchev *et al.* (TOTEM Collaboration), Europhys. Lett. **95**, 41001 (2011); G. Antchev *et al.* (TOTEM Collaboration), Europhys. Lett. **101**, 21002 (2013).
[31] K. A. Goulianos, Phys. Rep. **101**, 169 (1983).
[32] M. L. Good and W. D. Walker, Phys. Rev. **120**, 1857 (1960).
[33] V. A. Abramovsky, V. N. Gribov, and O. V. Kancheli, Yad. Fiz. **18**, 595 (1973) [Sov. J. Nucl. Phys. **18**, 308 (1974)].
[34] F. Oljemark and K. Osterberg (TOTEM Collaboration), LHC Student Poster Session, CERN Geneva 2013 (unpublished); F. Oljemark, EDS Blois Workshop, Saariselka, Lapland, 2013 (unpublished).
[35] A. Donnachie and P. V. Landshoff, Phys. Lett. B **296**, 227 (1992).
[36] V. A. Khoze, F. Krauss, A. D. Martin, M. G. Ryskin, and K. C. Zapp, Eur. Phys. J. C **69**, 85 (2010).
[37] A. B. Kaidalov, Sov. J. Nucl. Phys. **13**, 401 (1971).
[38] S. D. Drell and K. Hiida, Phys. Rev. Lett. **7**, 199 (1961); R. T. Deck, Phys. Rev. Lett. **13**, 169 (1964).
[39] A. Babaev, G. Eliseev, and V. Lubimov, Nucl. Phys. **B116**, 28 (1976).
[40] C. Patrignani *et al.*, Chin. Phys. C **40**, 100001 (2016).
[41] J. Engler *et al.*, Nucl. Phys. **B84**, 70 (1975).
[42] W. Flauger and F. Mönnig, Nucl. Phys. **B109**, 347 (1976).
[43] L. A. Ponomarev *et al.*, Yad. Phys. **22**, 807 (1975).
[44] M. G. Albrow, A. De Roeck, V. A. Khoze, J. Lämsä, E. Norbeck, Y. Onel, R. Orava, A. Penzo, and M. G. Ryskin, J. Instrum. **4**, P10001 (2009).